ARTICLES
https://doi.org/10.1038/s41561-019-0383-x
nature geoscience

Opposite tropical circulation trends in climate models and in reanalyses

Rei Chemke[1*] and Lorenzo M. Polvani[1,2]

The Hadley circulation has large climate impacts at low latitudes by transferring heat and moisture between the tropics and subtropics. Climate projections show a robust weakening of the Northern Hemisphere Hadley circulation by the end of the twenty-first century. Over the past several decades, however, atmospheric reanalyses indicate a strengthening of the Hadley circulation. Here we show that the strengthening of the circulation in the Northern Hemisphere is not seen in climate models; instead, these models simulate a weakening of the circulation in the past 40 years. Using observations and a large ensemble of model simulations we elucidate this discrepancy between climate models and reanalyses, and show that it does not stem from internal climate variability or biases in climate models, but appears related to artefacts in the representation of latent heating in the reanalyses. Our results highlight the role of anthropogenic emissions in the recent slowdown of the atmospheric circulation, which is projected to continue in coming decades, and question the reliability of reanalyses for estimating trends in the Hadley circulation.

The Hadley circulation (HC) comprises an ascending branch of warm and moist air around the equator, which condenses at the upper levels of the troposphere, flowing poleward at the upper levels with a descending branch of dry air in the subtropics, which returns equatorward near the surface. The transport of heat and moisture by this circulation plays an important role in setting low-latitude precipitation and temperature patterns: it acts to homogenize the temperature in the tropics and results in a high precipitation around the equator and low precipitation in the subtropics[1,2]. Climate projections robustly show a weakening of the Northern Hemisphere HC by the end of the twenty-first century, with significant impacts on low-latitude climate[3–5]. Different studies argue for different drivers of the projected weakening of the circulation: changes in the hydrological cycle[3,6], upper troposphere convective and radiative heating[7–9], temperature gradients[10–13] and eddy momentum fluxes[14,15].

Recent trends in Hadley cell strength

Has such a weakening already emerged? To answer this question, we start by examining the 39-year trends (1979–2017) of the annual mean Northern Hemisphere HC strength (Ψ_{max} (equation (1))) in 40 models of phase 5 of the Coupled Model Intercomparison Project (CMIP5) multimodel ensemble[16]. Each CMIP5 simulation was forced following the historical (twentieth century) and the Representative Concentration Pathway 8.5 (RCP8.5, twenty-first century) specifications. The CMIP5 trends are compared to the 39-year trends in five different reanalyses (ECMWF Era-Interim, NCEP/DOE Reanalysis II, JRA-55, MERRA-2 and CFSR V2) (Methods). In 35 out of 40 models, Ψ_{max} decreased over the past 39 years (blue bars in Fig. 1a). The multimodel mean (purple bar) shows a weakening of $-6.8\times10^{7}\,kg\,s^{-1}\,yr^{-1}$. In contrast, all five reanalyses show an increase in Ψ_{max} over the same period[17–24] (green bars in Fig. 1a). This inconsistency between the CMIP5 models and the reanalyses (which occurs across the HC, and not only in its maximum value (Supplementary Fig. 1)) is also clearly seen in the time series of Ψ_{max} (Fig. 1c). Although the CMIP5 models show a weakening of the circulation over the past few decades and throughout the entire twenty-first century, all the reanalyses show a strengthening in recent decades (these results are similar for the winter season (Supplementary Fig. 2), but the annual mean allows for better statistics). We focus here on the Northern Hemisphere HC, as in the Southern Hemisphere there are no robust trends in climate models over the past four decades and throughout the twenty-first century, and the trends in the reanalyses are consistent with those in the climate models (Supplementary Fig. 3).

This discrepancy between climate models and two reanalyses was documented over the past two decades of the twentieth century, and was argued to stem from the opposite trends in static stability in the middle–upper tropical troposphere (that is, warming in the models versus cooling in the reanalyses)[19]. Here we revisit this discrepancy, corroborate its existence (as shown above) and explicitly elucidate its origin by analysing a longer time record (39 years of data), five different reanalyses, 40 CMIP5 models and one large ensemble (LE) of model simulation, which allows disentangling the system's internal variability from its forced response to anthropogenic emissions, as discussed below. Although here we focus on the discrepancy in Ψ_{max} trends, recent simulated trends in the HC width do capture the trends from the reanalyses[25].

The role of internal variability in the Hadley cell trends

A few models do show a minor increase in Ψ_{max}, which might suggest that the discrepancy between the models and the reanalyses stems from internal variability. Owing to the chaotic nature of the climate system, the transient evolution of Ψ_{max} is sensitive to the initial conditions of each model. Thus, different initial conditions in the CMIP5 models might lead to both positive and negative trends of Ψ_{max}, which may then capture the positive trends in the reanalyses. To evaluate the role of internal variability in the discrepancy between the CMIP5 models and the reanalyses, we make use of a LE of model simulations[26]. The LE was computed with the Community Earth System Model (CESM1), and comprises 40 members integrated from 1920 to 2100 under the historical and RCP8.5

[1]Department of Applied Physics and Applied Mathematics, Columbia University, New York, NY, USA. [2]Department of Earth and Environmental Sciences, and Lamont-Doherty Earth Observatory, Columbia University, Palisades, NY, USA. *e-mail: rc3101@columbia.edu

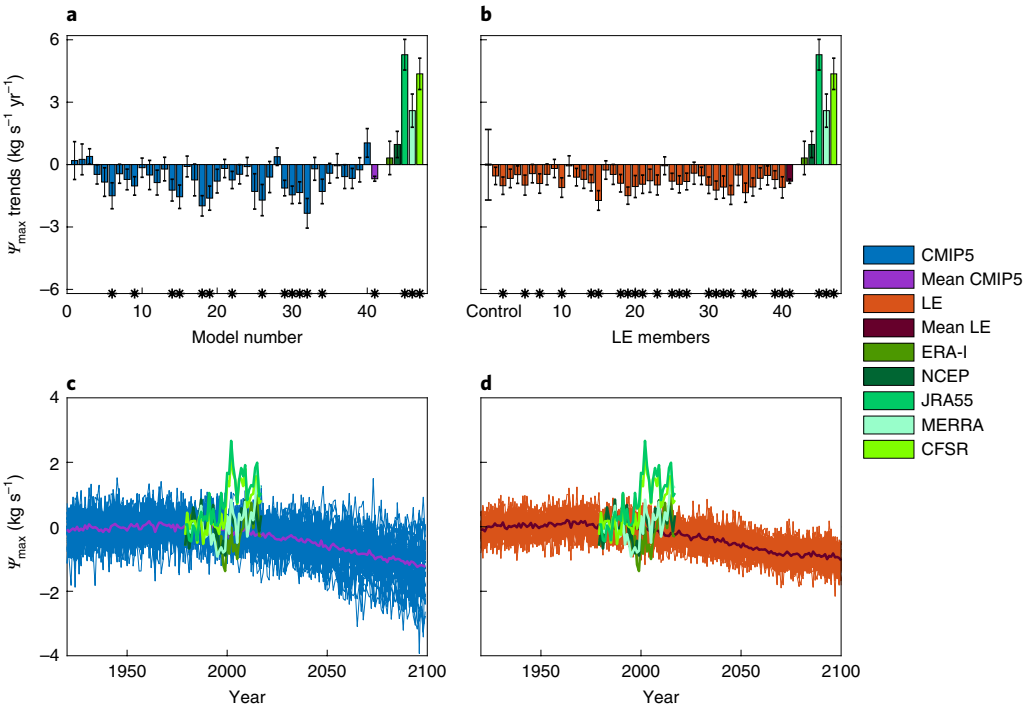

Fig. 1 | The 39-year (1979–2017) trends (10^8 kg s^{-1} yr^{-1}) and time series (10^{10} kg s^{-1}) of Ψ_{max}. **a**, Trends in CMIP5 models (blue bars) and their multimodel mean (purple bar). **b**, Trends in LE members (red bars) and their mean (maroon bar). The leftmost bar shows the internal variability of 39-year trends calculated from the preindustrial control CESM1 run. **c**, Time series of Ψ_{max} in CMIP5 models (blue bars) and their multimodel mean (purple bar). **d**, Time series of Ψ_{max} in LE models (red bars) and their mean (maroon bar). The time series are relative to the 1979–1989 period. In all the panels, green represents reanalyses. The trends from MERRA-2 are available from 1980. The asterisks in **a** and **b** show that the trends are statistically significant (*P* values lower than 0.1), and the error bars show the standard error of the linear regression coefficient.

scenarios, but with slightly different initial conditions (Methods). As for most CMIP5 models, all the LE members show a decrease in Ψ_{max} in recent decades (red bars in Fig. 1b), with a mean value of -7.9×10^7 kg s^{-1} yr^{-1} (maroon bar), attesting that internal variability cannot explain the positive trends in the reanalyses. The inability of internal variability to capture the increase in Ψ_{max} can be further seen by comparing the time series of all the LE members, which shows a decline through the twenty-first century, with the positive trends in the reanalyses (Fig. 1d).

Studying the Hadley cell using the Kuo–Eliassen equation

We can think of two other possible explanations for the above discrepancy. The first is that biases in the assimilation of observational data in reanalyses (from satellites and radiosondes), or deficiencies in the models used in the reanalyses[23,24], result in spurious positive trends of Ψ_{max}, and thus are inconsistent with the CMIP5 models. The second is that deficiencies in the physical and numerical formulations or in the external forcings used in climate models result in unrealistic negative trends of Ψ_{max}. We explore these alternative possibilities next by elucidating which physical processes control the behaviour of Ψ_{max} in both reanalyses and models.

This is done by solving the Kuo–Eliassen (KE) equation for the mean meridional streamfunction Ψ. The KE equation is derived using quasi-geostrophic approximation and thermal wind balance[27,28] (equation (2)), and takes the simple form, $L\Psi = D_Q + D_{\overline{v'T'}} + D_{\overline{u'v'}} + D_X$, where L is a second-order linear operator, which is a function of the Coriolis parameter and static stability. From the KE equation, one can see that the circulation, Ψ, is controlled by four physical processes: diabatic heating (D_Q), meridional eddy heat fluxes ($D_{\overline{v'T'}}$), the meridional eddy momentum fluxes ($D_{\overline{u'v'}}$) and the zonal friction (D_X) (Methods). We solved the KE equation for Ψ for each year using a successive over-relaxation method, with the terms on the right-hand side (RHS) specified from all the reanalyses with the available diabatic heating and eddy fluxes, and from all LE members. The LE is used because, first, it shows a weakening of Ψ_{max} (and is thus representative of most CMIP5 models), second, it allows us to examine further the role of internal variability and, third, all the model output needed to solve the KE equation is available. Although an analysis based on one model might be biased towards the model's formulations, most of the Ψ_{max} weakening trend variability across the CMIP5 models stems from internal variability and not from the different model formulations (73% of the variability is captured by the LE). The HC obtained by solving the KE equation (denoted Ψ^{KE}) is very close to the actual streamfunction (Ψ (Supplementary Fig. 4)). Moreover, the interannual variability (Supplementary Fig. 5) and the trends obtained from solving the KE equation (Ψ^{KE}_{max}) over the past 39 years are highly correlated with the actual Ψ_{max} interannual variability and trends (trend correlation of 0.98 for LE plus reanalyses and of 0.91 for LE alone (Fig. 2a)). This excellent agreement gives us confidence that the KE equation is a good tool to understand the origin of the discrepancy between models and reanalyses.

As the KE equation is linear, we next examine the separate contributions of changes in each of the RHS terms, plus changes in static stability S^2 (which appears in L) to changes in Ψ^{KE}_{max} (equation (4)); the total trends, and the individual contributions, are shown in Fig. 2b. The term that mostly contributes to the discrepancy between the LE and the reanalyses is diabatic heating (D_Q), which is responsible for the strengthening of the HC in all the reanalyses. This result is not sensitive to the method used to estimate diabatic heating (the thermodynamic equation residual versus the model produced (Supplementary Fig. 6)). The other terms either do not contribute to

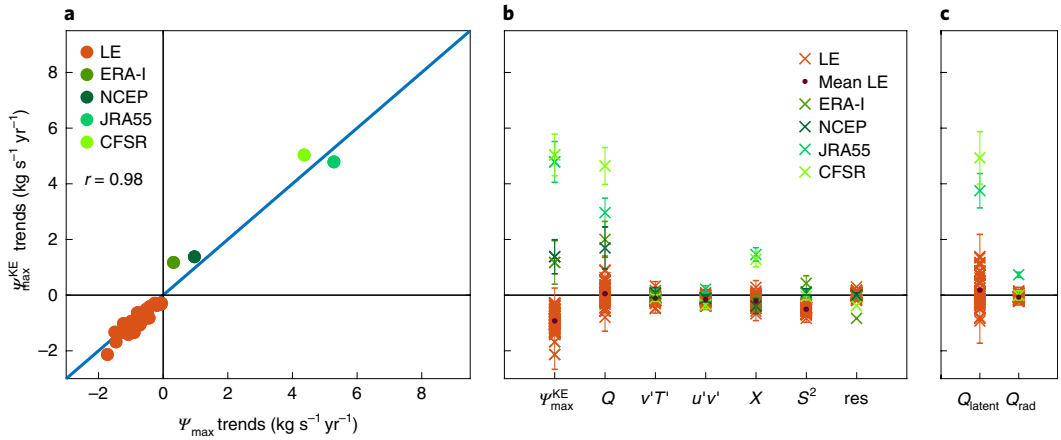

Fig. 2 | The 39-year (1979–2017) trends (10^8 kg s^{-1} yr^{-1}) of the Northern Hemisphere HC strength calculated from the KE equation Ψ^{KE}_{max}. **a**, Trends based on the solution of the KE equation (Ψ^{KE}_{max} (equation (2))) as a function of the streamfunction trends (Ψ_{max} (computed from equation (1))). The correlation between the trends is $r = 0.98$. **b**, The relative contributions to the trends of the solution of the KE equation (Ψ^{KE}_{max} (equation (4))) from diabatic heating (Q), eddy heat fluxes ($v'T'$), eddy momentum fluxes ($u'v'$), zonal friction (X), static stability (S^2) and the residual. **c**, The decomposition of Q to Q_{latent} and Q_{rad} heating. The trends in **c** are based on 32 (1979–2010) years. Error bars show the standard error of the linear regression coefficient. In all panels, orange represents the LE (mean LE in maroon) and green represents the reanalyses.

the discrepancy between the LE and reanalyses (for example, eddy heat and momentum fluxes), or show inconsistent trends across the reanalyses (for example, zonal friction). Note that although diabatic heating is the largest contributor to the strengthening in the reanalyses, its effect can be partly masked by other terms (which, for example, results in a minor strengthening of Ψ_{max} in ERA-I (Fig. 1a)). Unlike previous studies that, after examining the vertical structure of temperature changes, suggested static stability is important to explain the discrepancy between climate models and reanalyses[19,29], we here show, by quantifying the static stability contribution to Ψ_{max} using the KE equation, that it seems to play only a secondary role. Our different results might stem from the different time periods used for the analyses, and from the fact that previous studies did not actually quantify the effect of static stability and compared it to the effects of other processes (for example, diabatic heating and eddy fluxes). In fact, tropical mid-troposphere trends of static stability, which were suggested to explain the discrepancy between climate models and reanalyses, have the same sign across the CMIP5 models and three different reanalyses (Supplementary Fig. 7), and thus cannot explain the discrepancy. Although we cannot fully elucidate the mechanism behind the simulated weakening of Ψ_{max}, we do find that static stability plays an important role in the weakening of Ψ_{max} over the past few decades (Fig. 2b), as also suggested in previous studies for the projected weakening and widening of the tropical circulations[7,10,30,31].

The contribution of diabatic heating can be further separated into contributions from latent heat release (Q_{latent}) and radiative (Q_{rad}) heating. The full latitude–height structure of these variables is available for the LE and in two reanalyses (CFSR and JRA55), but not for all 39 years (Methods). Thus, for a proper comparison, only the 32 overlapping years (1979–2010) between the LE and reanalyses are analysed. This analysis further shows that most of the discrepancy in diabatic heating stems from Q_{latent} (Fig. 2c) (using the whole 35 years in JRA55 shows the same results). Although the Q_{latent} term is only available in two reanalyses, these reanalyses include the largest trends of Ψ_{max}, which allows for an easier identification of the origin of the discrepancy between climate models and reanalyses.

Validating Q_{latent} trends with observations

We explore the source of the discrepancy by examining the latitudinal structure of Q_{latent} in the reanalyses and LE. As seen in Fig. 3a, the vertically integrated Q_{latent} trends show that the largest discrepancy is around the equator, where the reanalyses show larger positive trends in Q_{latent}. To assess which data, the reanalyses or the models, might have an erroneous representation of Q_{latent} (which eventually results in the opposite trends of Ψ_{max}), we compare the precipitation trends in the models and the reanalyses with precipitation trends from the Global Precipitation Climatology Project (GPCP) (Methods). Surface precipitation can be used as a proxy for the net Q_{latent} in an atmospheric column. The GPCP data are constructed from satellite and gauge observation, and are uncontaminated from potential model or assimilation errors—this allows us to ascertain how realistic the Q_{latent} trends in models and reanalyses are. As seen in Fig. 3b, similar to the Q_{latent} trends, the precipitation trends in the reanalyses show larger values around the equator than for the LE (Fig. 3b). Although here we study the two reanalyses for which Q_{latent} is available, similar strong precipitation trends at low latitudes are found in all the reanalyses except ERA-I, which is consistent with its smaller trends of Ψ_{max} (Supplementary Fig. 8). The observed GPCP trends at low latitudes agree with the LE trends but not with the reanalyses trends, which implies a deficiency in Q_{latent} trends in the reanalyses. Similarly, precipitation in CMIP5 models agrees with that in GPCP (Fig. 3c), which further highlights that climate models do capture the observed precipitation.

We thus conclude that the positive trends in Ψ_{max} in the reanalyses are likely to be an artefact. Although this artefact is present in all the reanalyses, its magnitude varies across the different products mostly due to internal variability: the variability across the reanalyses ($\sigma = 2.1 \times 10^8$ kg s^{-1} yr^{-1}) is within the range of internal variability (3.4×10^8 kg s^{-1} yr^{-1}, estimated from the CESM1 preindustrial control run (Fig. 1b)). The origin of this artefact is unclear at present. Recently, the lack of mass conservation in the early generation of the reanalyses was invoked to explain the weaker trend in HC expansion in the models versus the reanalyses[32]. Although the lack of mass conservation may also bias the Ψ_{max} trends in the reanalyses reported above, here we analysed the new generation of reanalyses, which have improved their mass conservation, so mass conservation is unlikely be the primary reason for the discrepancy between models and reanalyses. The inclusion of new satellite data around the year 2000 might also affect the bias in the reanalyses, but is not necessarily the main reason; although two reanalyses (CFSR

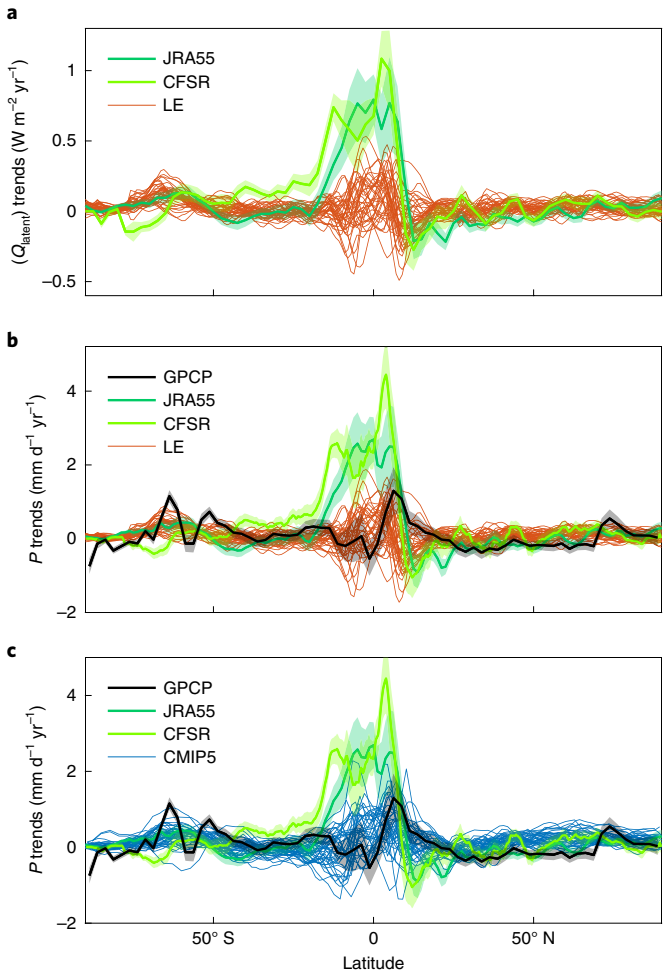

Fig. 3 | The 32-year (1979–2010) Q_{latent} (W m^{-2} yr^{-1}) and precipitation (10^{-2} mm d^{-1} yr^{-1}) trends. a, Vertically integrated Q_{latent} trends. **b**,**c**, Precipitation trends. Green lines, reanalyses; red lines, LE; blue lines, CMIP5. In **b** and **c** the black line represents the GPCP trends. The shading shows the standard error of the linear regression coefficient.

and JRA55) show strong trends mostly prior to year 2000, the other three reanalyses (ERA-I, NCEP and MERRA-2) show strong trends mostly after year 2000 (Fig. 1c).

As Q_{latent} is strongly coupled to surface temperature, one might be tempted to relate the discrepancy in Ψ_{max} trends between models and reanalyses to the recent 'slowdown' in surface and tropospheric warming[33]. However, analysing the CESM1 LE 'Pacemaker' runs[34] (Methods), which by nudging eastern tropical Pacific sea surface temperature anomalies to the observations captures the recent warming hiatus[35], shows that the discrepancy between models and reanalyses remains: between 1979 and 2013, Ψ_{max} weakens in most pacemaker runs (especially in those runs that best capture the observed pattern of surface air temperature trends), with a mean value of -3.6×10^{7} kg s^{-1} yr^{-1}, whereas most reanalyses show a strengthening (Supplementary Fig. 9).

Our results not only explain the discrepancy in the HC strength trends between climate models and reanalyses, but also show that the weakening of the HC over the past ~40 years, simulated by models, is part of the forced response to anthropogenic emissions, and not a manifestation of internal variability: all the LE members show a decline in Ψ_{max} in recent years, and the decline is projected to continue in the coming decades (Fig. 1b). The inability of the reanalyses to capture the weakening of the HC over the past ~40 years raises issues as to their use as an observational estimate for HC strength trends. However, it is important to keep in mind that for many other multidecadal atmospheric trends the reanalyses agree well with climate models (for example, the widening of the HC[25], weakening of boreal summer monsoon overturning circulation[30,36] and so on).

Online content

Any methods, additional references, Nature Research reporting summaries, source data, statements of code and data availability and associated accession codes are available at https://doi.org/10.1038/s41561-019-0383-x.

Received: 3 January 2019; Accepted: 9 May 2019;
Published online: 24 June 2019

References

1. Vallis, G. K. *Atmospheric and Oceanic Fluid Dynamics* (Cambridge Univ. Press, 2006).
2. Hartmann, D. L. *Global Physical Climatology* 2nd edn (Academic, 2016).
3. Vecchi, G. A. & Soden, B. J. Global warming and the weakening of the tropical circulation. *J. Clim.* **20**, 4316–4340 (2007).
4. Kang, S. M., Deser, C. & Polvani, L. M. Uncertainty in climate change projections of the Hadley circulation: the role of internal variability. *J. Clim.* **26**, 7541–7554 (2013).
5. Vallis, G. K., Zurita-Gotor, P., Cairns, C. & Kidston, J. Response of the large-scale structure of the atmosphere to global warming. *Q. J. R. Meteorol. Soc.* **141**, 1479–1501 (2015).
6. Held, I. M. & Soden, B. J. Robust responses of the hydrological cycle to global warming. *J. Clim.* **19**, 5686–5699 (2006).
7. Knutson, T. R. & Manabe, S. Time-mean response over the tropical Pacific to increased CO_2 in a coupled ocean–atmosphere model. *J. Clim.* **8**, 2181–2199 (1995).
8. Bony, S. et al. Robust direct effect of carbon dioxide on tropical circulation and regional precipitation. *Nat. Geosci.* **6**, 447–451 (2013).
9. Merlis, T. M. Direct weakening of tropical circulations from masked CO_2 radiative forcing. *Proc. Natl Acad. Sci. USA* **112**, 13167–13171 (2015).
10. Gastineau, G., Le Treut, H. & Li, L. Hadley circulation changes under global warming conditions indicated by coupled climate models. *Tellus* **60**, 863–884 (2008).
11. Gastineau, G., Li, L. & Le Treut, H. The Hadley and Walker circulation changes in global warming conditions described by idealized atmospheric simulations. *J. Clim.* **22**, 3993–4013 (2009).
12. Ma, J., Xie, S.-P. & Kosaka, Y. Mechanisms for tropical tropospheric circulation change in response to global warming. *J. Clim.* **25**, 2979–2994 (2012).
13. Seo, K.-H., Frierson, D. M. W. & Son, J.-H. A mechanism for future changes in Hadley circulation strength in CMIP5 climate change simulations. *Geophys. Res. Lett.* **41**, 5251–5258 (2014).
14. Schneider, T., O'Gorman, P. A. & Levine, X. J. Water vapor and the dynamics of climate change. *Rev. Geophys.* **48**, RG3001 (2010).
15. Levine, X. J. & Schneider, T. Response of the Hadley circulation to climate change in an aquaplanet GCM coupled to a simple representation of ocean heat transport. *J. Atmos. Sci.* **68**, 769–783 (2011).
16. Taylor, K. E., Stouffer, R. J. & Meehl, G. A. An overview of CMIP5 and the experiment design. *Bull. Am. Meteorol. Soc.* **93**, 485–498 (2012).
17. Quan, X. W., Diaz, H. F. & Hoerling, M. P. in *The Hadley Circulation: Past, Present and Future* (eds Diaz, H. F. & Bradley, R. S.) 85–120 (Kluwer Academic, 2004).
18. Mitas, C. M. & Clement, A. Has the Hadley cell been strengthening in recent decades? *Geophys. Res. Lett.* **32**, L03809 (2005).
19. Mitas, C. M. & Clement, A. Recent behavior of the Hadley cell and tropical thermodynamics in climate models and reanalyses. *Geophys. Res. Lett.* **33**, L01810 (2006).
20. Song, H. & Zhang, M. Changes of the boreal winter Hadley circulation in the NCEP–NCAR and ECMWF reanalyses: a comparative study. *J. Clim.* **20**, 5191–5200 (2007).
21. Stachnik, J. P. & Schumacher, C. A comparison of the Hadley circulation in modern reanalyses. *J. Geophys. Res.* **116**, D22102 (2011).
22. Liu, J., Song, M., Hu, Y. & Ren, X. Changes in the strength and width of the Hadley circulation since 1871. *Climate* **8**, 1169–1175 (2012).
23. Nguyen, H., Evans, A., Lucas, C., Smith, I. & Timbal, B. The Hadley circulation in reanalyses: climatology, variability, and change. *J. Clim.* **26**, 3357–3376 (2013).
24. D'Agostino, R. & Lionello, P. Evidence of global warming impact on the evolution of the Hadley circulation in ECMWF centennial reanalyses. *Clim. Dyn.* **48**, 3047–3060 (2017).

25. Grise, K. M. et al. Recent tropical expansion: natural variability or forced response? *J. Clim.* **32**, 1551–1571 (2019).
26. Kay, J. E. et al. The community earth system model (CESM) large ensemble project: a community resource for studying climate change in the presence of internal climate variability. *Bull. Am. Meteorol. Soc.* **96**, 1333–1349 (2015).
27. Kuo, H.-L. Forced and free meridional circulations in the atmosphere. *J. Atmos. Sci.* **13**, 561–568 (1956).
28. Peixoto, J. P. & Oort, A. H. *Physics of Climate* (American Institute of Physics, 1992).
29. Sohn, B.-J., Lee, S., Chung, E.-S. & Song, H.-J. The role of the dry static stability for the recent change in the Pacific Walker circulation. *J. Clim.* **29**, 2765–2779 (2016).
30. Krishnan, R. et al. Will the South Asian monsoon overturning circulation stabilize any further? *Clim. Dyn.* **40**, 187–211 (2013).
31. Chemke, R. & Polvani, L. M. Exploiting the abrupt $4 \times CO_2$ scenario to elucidate tropical expansion mechanisms. *J. Clim.* **32**, 859–875 (2019).
32. Davis, N. A. & Davis, S. M. Reconciling Hadley cell expansion trend estimates in reanalyses. *Geophys. Res. Lett.* **45**, 11,439–11,446 (2018).
33. IPCC *Climate Change 2013: The Physical Basis* (eds Stocker, T. F. et al.) 1–29 (Cambridge Univ. Press, 2013).
34. Deser, C., Guo, R. & Lehner, F. The relative contributions of tropical Pacific sea surface temperatures and atmospheric internal variability to the recent global warming hiatus. *Geophys. Res. Lett.* **44**, 7945–7954 (2017).
35. Kosaka, Y. & Xie, S. P. Recent global-warming hiatus tied to equatorial Pacific surface cooling. *Nature* **501**, 403–407 (2013).
36. Sooraj, K. P., Terray, P. & Mujumdar, M. Global warming and the weakening of the Asian summer monsoon circulation: assessments from the CMIP5 models. *Clim. Dyn.* **45**, 233–252 (2015).

Acknowledgements

Supported by the NOAA Climate and Global Change Postdoctoral Fellowship Program, which is administered by UCAR's Cooperative Programs for the Advancement of Earth System Science (CPAESS). L.M.P. is grateful for the continued support of the US Natural Science Foundation.

Author contributions

R.C. downloaded and analysed the data and, together with L.M.P., discussed and wrote the paper.

Competing interests

The authors declare no competing interests.

Additional information

Supplementary information is available for this paper at https://doi.org/10.1038/s41561-019-0383-x.

Reprints and permissions information is available at www.nature.com/reprints.

Correspondence and requests for materials should be addressed to R.C.

Publisher's note: Springer Nature remains neutral with regard to jurisdictional claims in published maps and institutional affiliations.

Methods

The Hadley cell strength. The strength of the Northern Hemisphere HC (Ψ_{max}) is defined as the maximum value of the streamfunction (Ψ):

$$\Psi(\phi,p)=\frac{2\pi a\cos\phi}{g}\int_0^p \bar{v}(\phi,p')\mathrm{d}p' \quad (1)$$

at 500 mbar, where ϕ is the latitude, p the pressure, a the Earth's radius, g is the gravitational acceleration, v the meridional wind, the overbar represents the zonal and annual mean and p' is a dummy pressure variable of integration.

CMIP5. Monthly mean data from 40 models from CMIP5[16] were used in this study, and are listed in Supplementary Table 1 (https://cmip.llnl.gov/cmip5/availability.html). All the models are under the 'r1i1p1' ensemble and forced with the historical forcing through 2005 and the RCP8.5 forcing through 2100.

Reanalyses. 1979–2017 monthly mean data from five different reanalyses, which constrain general circulation models (GCMs) to both satellite data and in-situ measurements, are used in this study:

1. The ECMWF Era-Interim (ERA-I)[37] with a 0.75° grid resolution (https://www.ecmwf.int).
2. NCEP/DOE Reanalysis II (ref. [38]) with a 2.5° grid resolution (https://www.esrl.noaa.gov/psd/data/gridded/data.ncep.reanalysis2.html).
3. JRA-55 (ref. [39]) with a 1.25° grid resolution (https://rda.ucar.edu/ and https://esgf.nccs.nasa.gov/projects/create-ip/).
4. MERRA-2 (ref. [40]) with a 0.5° grid resolution (https://rda.ucar.edu/ and https://esgf.nccs.nasa.gov/projects/create-ip/).
5. CFSR V2 (ref. [41]) with a 0.5° grid resolution (https://rda.ucar.edu/ and https://esgf.nccs.nasa.gov/projects/create-ip/).

LE simulations. To estimate the role of internal variability in the discrepancy between the Hadley cell strength trends in CMIP5 models and in reanalyses we make use of the CESM1 LE[26]. The LE data are available at http://www.cesm.ucar.edu/. The LE comprises a set of 40 members integrated from 1920 to 2100 under the historical scenario through 2005 and RCP8.5 scenario thereafter. Although all the members are subjected to the same forcing and are run with the same model, they differ in their initial conditions: the initialized air temperature randomly varies across the members by an order of 10^{-14} K. Owing to the chaotic nature of the climate system, a small change in the initial conditions leads to a distinct transient evolution of each member, and thus allows one to explore the range of internal variability. Taking the mean of all the members averages out the internal variability and yields the system's forced response. We also make use of the 1800-year long CESM1 preindustrial control run, in which the forcing is held fixed at year 1850. The constant forcing in that simulation allows one to quantify the internal variability in the unforced system.

Streamfunction equation. We solve the KE equation for the mean meridional streamfunction[27], Ψ, to elucidate the physical processes that contribute to the discrepancy in the Hadley cell strength trends between the CMIP5 models and the reanalyses. The KE equation is derived by combining the thermodynamic and momentum quasi-geostrophic equations using thermal wind balance (section 14.5.5 in Peixoto and Oort[28]), which yields, in spherical coordinates:

$$f^2\frac{g}{2\pi a\cos\phi}\frac{\partial^2\Psi}{\partial p^2}+S^2\frac{g}{2\pi a}\frac{\partial}{a\partial\phi}\frac{1}{a\cos\phi}\frac{\partial\Psi}{\partial\phi}$$
$$=\frac{R}{p}\left(\frac{1}{a}\frac{\partial\overline{Q}}{\partial\phi}-\frac{\partial}{a\partial\phi}\frac{1}{a\cos\phi}\frac{\partial\overline{v'T'}\cos\phi}{\partial\phi}\right)+f\left(\frac{1}{a\cos^2\phi}\frac{\partial^2\overline{u'v'}\cos^2\phi}{\partial p\partial\phi}-\frac{\partial\overline{X}}{\partial p}\right) \quad (2)$$

where f is the Coriolis parameter, $S^2=-\frac{1}{\rho\theta}\frac{\partial\theta}{\partial p}$ the static stability, ρ the density, θ the potential temperature, $R=287\,\mathrm{J\,kg^{-1}\,K^{-1}}$ (the gas constant of dry air), $\overline{Q}$ the diabatic heating, T the temperature, u the zonal wind, $\overline{v'T'}$ and $\overline{u'v'}$ the eddy heat and momentum fluxes, respectively, a prime represents deviation from zonal and monthly mean and $\overline{X}$ is the zonal friction. We numerically solved this equation with the RHS terms calculated from the LE and NCEP, ERA-I, JRA55 and CFSR reanalyses, using a successive over-relaxation method. The eddy fluxes and diabatic heating from the reanalyses were calculated using daily data. The diabatic heating was calculated using the thermodynamic equation, $Q=\frac{DT}{Dt}-\frac{\omega TR}{pc_p}$, where $\frac{D}{Dt}=\frac{\partial}{\partial t}+\mathbf{V}\cdot\nabla$, $\mathbf{V}=(u,v,\omega)$, ω is the vertical velocity, and $c_p=1{,}004\,\mathrm{J\,kg^{-1}\,K^{-1}}$ is the specific heat capacity. The zonal friction was estimated using the annual mean zonal momentum quasi-geostrophic equation, $\overline{X}=\frac{1}{a\cos^2\phi}\frac{\partial^2\overline{u'v'}\cos^2\phi}{\partial\phi^2}-f\overline{v}$. Latent and radiative heating from JRA55 and CFSR are available from 1979 to 2013 and to 2010, respectively.

The solution for equation (2), denoted Ψ^{KE}, is similar to the streamfunction calculated from equation (1), as shown in Supplementary Fig. 4, which compares Ψ and Ψ^{KE} in both the LE (member 10) and NCEP reanalysis at year 1979. Different years and different members of the LE also show a good agreement between Ψ and Ψ^{KE}. The 39-year interannual variability and trends of the Hadley cell strength from Ψ^{KE} (Ψ^{KE}_{max}) show good agreement with the interannual variability and trends of Ψ_{max}, with a very high correlation (trend correlation of $r=0.98$) (Fig. 2a and Supplementary Fig. 5). This give us confidence in using equation (2) to elucidate the processes that result in the discrepancy in the Hadley cell strength trends between the CMIP5 models and the reanalyses. Similar to Kim and Lee[42], elucidating this discrepancy is done by calculating the relative contribution to the trends in Ψ^{KE} from each of the terms in equation (2), which can then be rewritten:

$$L\Psi=D \quad (3)$$

where L is the linear operator on the left-hand side in equation (2), and D is the sum of the terms on the RHS of equation (2). One can decompose L, Ψ and D to their values at 1979 and a deviation from that year, $L=L_{1979}+\delta L$, $\Psi=\Psi_{1979}+\delta\Psi$ and $D=D_{1979}+\delta D$. Substituting these into equation (3) provides an equation for $\delta\Psi$:

$$L_{1979}\delta\Psi=\delta D-\delta L\Psi_{1979}-\delta L\delta\Psi \quad (4)$$

where the first term on the RHS represents changes in diabatic heating, eddy meridional heat and momentum fluxes, and zonal friction, the second term represents changes in static stability (the operator) and the third term is the multiplication between static stability and streamfunction changes (calculated as a residual). As the annual mean streamfunction is analysed, the system is closed to its steady-state solution and the different terms in the streamfunction equation are not independent. Thus, the contribution of each term does not necessarily stem from a direct response to the forcing, but may stem from changes in the other terms[42]. The changes are defined relative to 1979 because this is the first year available from the reanalyses. Note, however, that as we are studying the trends in Ψ^{KE} the choice of this year does not affect the results.

Precipitation (GPCP). The observed precipitation between 1979 and 2017 is taken from the GPCP[43], available at https://www.esrl.noaa.gov/psd/data/gridded/data.gpcp.html. The GPCP provides monthly mean precipitation, with a 2.5° grid resolution, by integrating satellite, gauge and sounding data.

Pacemaker runs. As shown in previous studies[34,35], by nudging sea surface temperature anomalies to observations, the Pacemaker runs are able to capture the recent slowdown in surface warming. These runs are conducted using the CESM1[44] under the historical scenario through 2005 and the RCP8.5 scenario through 2013. In the tropical east Pacific (15° S to 15° N), the sea surface temperature anomalies are nudged to observations based on the NOAA Extended Reconstruction Sea Surface Temperature version 3 (details in Deser et al.[34]). Here we analysed a ten-member LE of the CESM1 Pacemaker simulations through 1979–2013 to account for the role of internal variability, which was found to be significant in capturing the observed pattern of temperature trends. Similar to Fig. 1, most members still show a small weakening of the Hadley cell strength, even by nudging the eastern tropical Pacific temperature to observations, whereas reanalyses show a strengthening over the same period (Supplementary Fig. 9). There is a low and negative correlation of $r=-0.39$ between the Hadley cell strength trends in the Pacemaker runs and the pattern correlation of the surface air temperature in the Pacemaker runs and the observed surface air temperature (Deser et al.[34]). Thus, members that show the highest pattern correlation with the observed surface temperature show the largest weakening of the circulation.

Data availability

The data used in the manuscript are publicly available for CMIP5 data (https://esgf-node.llnl.gov/projects/cmip5/), LE (http://www.cesm.ucar.edu/), ERA-I (https://www.ecmwf.int), NCEP2 (https://www.esrl.noaa.gov/psd/data/gridded/data.ncep.reanalysis2.html), JRA55, MERRA-2 and CFSR2 (https://rda.ucar.edu/ and https://esgf.nccs.nasa.gov/projects/create-ip/) and GPCP (https://www.esrl.noaa.gov/psd/data/gridded/data.gpcp.html).

Code availability

The code for calculating the KE equation is available upon request from rc3101@columbia.edu.

References

37. Dee, D. P. et al. The ERA-Interim reanalysis: configuration and performance of the data assimilation system. *Q. J. R. Meteorol. Soc.* **137**, 553–597 (2011).
38. Kanamitsu, M. et al. NCEP–DOE AMIP-II reanalysis (R-2). *Bull. Am. Meteorol. Soc.* **83**, 1631–1643 (2002).
39. Kobayashi, S. et al. The JRA-55 reanalysis: general specifications and basic characteristics. *J. Meteorol. Soc. Jpn* **93**, 5–48 (2015).
40. Gelaro, R. et al. The modern-era retrospective analysis for research and applications, version 2 (MERRA-2). *J. Clim.* **30**, 5419–5454 (2017).
41. Saha, S. et al. The NCEP climate forecast system version 2. *J. Clim.* **27**, 2185–2208 (2014).
42. Kim, H.-K. & Lee, S. Hadley cell dynamics in a primitive equation model. Part I: axisymmetric flow. *J. Atmos. Sci.* **58**, 2845–2858 (2001).
43. Adler, R. F. et al. The version-2 global precipitation climatology project (GPCP) monthly precipitation analysis (1979–present). *J. Hydrometeor* **4**, 1147–1167 (2003).
44. Hurrell, J. W. et al. The Community Earth System Model: a framework for collaborative. *Res. Bull. Am. Meteorol. Soc.* **94**, 1339–1360 (2013).